INTERNATIONAL JOURNAL FOR NUMERICAL METHODS IN FLUIDS
Int. J. Numer. Meth. Fluids 2004; **46**:1–18 (DOI: 10.1002/fld.745)

Numerical methods for large-eddy simulation in general co-ordinates

Gefeng Tang, Zhiyin Yang*,† and James J. McGuirk

Department of Aeronautical and Automotive Engineering, Loughborough University, Loughborough LE11 3TU, U.K.

SUMMARY

Large scale unsteady motions in many practical engineering flows play a very important role and it is very unlikely that these unsteady flow features can be captured within the framework of Reynolds averaged Navier–Stokes approach. Large-eddy simulation (LES) has become, arguably, the only practical numerical tool for predicting those flows more accurately since it is still not realistic to apply DNS to practical engineering flows with the current and near future available computing power.

Numerical methods for the LES of turbulent flows in complex geometry have been developed and applied to predict practical engineering flows successfully. The method is based on body-fitted curvilinear co-ordinates with the contravariant velocity components of the general Navier–Stokes equations discretized on a staggered orthogonal mesh. For incompressible flow simulations the main source of computational expense is due to the solution of a Poisson equation for pressure. This is especially true for flows in complex geometry. A multigrid 3D pressure solver is developed to speed up the solution. In addition, the Poisson equation for pressure takes a simpler form with no cross-derivatives when orthogonal mesh is used and hence resulting in increased convergence rate and producing more accurate solutions. Copyright © 2004 John Wiley & Sons, Ltd.

KEY WORDS: large-eddy simulation; Poisson equation; multigrid

1. INTRODUCTION

Large-eddy simulation, confined at the early stage to very simple configurations such as isotropic homogeneous turbulence, plane channel flows and flat plate boundary layer transition [1–3], has been undergoing a blooming development and matured to the point where application to complex flows is desirable. It has been applied more and more to study the physical phenomena that occur in engineering-like applications such as separated flows [4, 5], rotating pipe flows [6, 7], flow over blunt bodies [8] and mixing and swirling jet flows [9]. However, most of these LES works have been performed in relatively simple geometry. LES of realistic engineering flows in complex geometry is scarce and still a big challenge because

*Correspondence to: Zhiyin Yang, Department of Aeronautical and Automotive Engineering, Loughborough University, Loughborough LE11 3TU, U.K.
†E-mail: z.yang@lboro.ac.uk

Published online 15 June 2004
Received 21 June 2003
Revised 16 April 2004

it requires reliable, robust, accurate, efficient numerical methods to solve the 3D governing equations in general curvilinear co-ordinates in addition to sub-grid scale modelling.

This paper describes the development of a finite volume code for performing LES of practical engineering flows in complex geometry and discusses related numerical issues such as filtering, choice of velocity components: Cartesian or contravariant, staggered or non-staggered grids. Sub-grid scale modelling will not be addressed in this paper and can be found elsewhere [10].

The code has been applied to practical complicated engineering flows. The simulated results compare well with the available experimental data which demonstrates that the numerical methods are reliable and robust.

2. MATHEMATICAL FORMULATION

2.1. Governing equations

To develop numerical methods for the incompressible Navier–Stokes equations in general curvilinear co-ordinates the following choices have first to be made: (i) velocity components: Cartesian, contravariant or other; (ii) a staggered or non-staggered grid. These two issues are not totally independent and will be briefly discussed here.

Discretization on a non-staggered grid in general co-ordinates are less complicated than on a staggered grid. However, it is established from RANS calculation that with non-staggered grids artificial stabilizing terms (pressure smoothing) are required. It is not clear how big the effects can be and what the best way is to treat 'pressure smoothing' in the case of LES since so far little work has been reported to demonstrate this point. Staggered grids easily lead to inherently stable and accurate discretization and have been widely used in the LES community, especially due to the fact that conservative property can be achieved on a staggered grid, for example with second-order central differencing [11]. Hence a staggered grid is employed in the current study and numerical results for turbulent flow in a 180° bend duct will be compared with those obtained by a LES code using a collocated grid.

If contravariant velocity components are used, additional body force terms arise due to grid line curvature. In these terms the so-called Christoffel symbols occur which involve the second derivatives of the co-ordinate mapping so that inaccuracies are to be feared on non-smooth grids. Many researchers prefer to use Cartesian velocity components to avoid the Christoffel symbols for this reason, and for another reason of huge memory requirements because there are so many of them (18 in three dimensions) and plus other geometric metrics, transformation matrix. Some of them need to be stored at several positions of the staggered mesh so that the memory requirement is huge. However, Cartesian velocity components do not combine easily with staggered grids in general co-ordinates because the Cartesian velocity components are not normal to co-ordinate lines. To avoid the excessive requirement of storage space the transformation in the current study is restricted to x and y (2D) and in the third dimension (z) the grid can be either translated or rotated by which many complicated practical engineering geometries, especially in gas turbine engine, can be represented. This is a step forward compared with the numerical methods developed by Yang and Voke [12] which can only allow translation in the third dimension. In addition, orthogonal grid (in practice it is very difficult to generate the orthogonal grid everywhere but extreme care has been taken

to ensure that the grid in the present study is orthogonal or very close to orthogonal) is employed in the current study so that the equations can be further simplified, especially there will be no cross-derivative terms in the Poisson equation for pressure which will speed up the convergence and possibly increase the accuracy.

Details of the mathematical transformation of the governing equations can be found elsewhere [13] and the governing equations of incompressible flows may be written in following form:

$$\nabla(i)[V_i] = 0 \tag{1}$$

$$\frac{\partial}{\partial t}(V_j) + \nabla(i)[V_i V_j + \tau_{ij}] = -\frac{\partial P}{\partial x(j)} + H_i(j)[V_i V_j + \tau_{ii}] - H_i(j)[V_i V_i + \tau_{ij}] \tag{2}$$

$$\tau_{ij} = -\upsilon_e \left(\frac{\partial V_i}{\partial x(j)} + \frac{\partial V_j}{\partial x(i)} - V_i H_i(j) - V_j H_j(i) + 2\delta_{ij} V_m H_j(m) \right)$$

where V_j are the contravariant velocity components. $\nabla(i)$ is the divergence operator and $H_i(j)$ is the co-ordinate variation terms, defined as

$$H_i(j) = \frac{1}{h_i} \frac{\partial h_i}{\partial x(j)} \tag{3}$$

$$\nabla(i) = \frac{h_i}{|h|} \frac{\partial}{\partial x(i)} \left[\frac{|h|}{h_i} \right] \tag{4}$$

in which $h_i = \sqrt{g_{ii}}$ is the scale factors and $|h|$ is the product of the scale factors representing the volume ratio between the co-ordinate systems. Note that $x(i)$ is not a co-ordinate system but a notational convenience and the curvilinear orthogonal system x^i is related to $x(i)$ as follows:

$$x(i) = h_i x^i \tag{5}$$

In Equation (2), υ_e is the sum of molecular viscosity and the sub-grid eddy-viscosity which is obtained through the Smagorinsky SGS model [14] with the van Driest Damping function in the present study. The Smagorinsky constant is 0.1 for all the cases in the present study.

All the geometric quantities can be calculated from the input co-ordinates data of the cell-vertices (grid nodes) once for all at the beginning. The process is briefly described below.

As mentioned before that in the current study the 3D grids are generated by either translating or rotating the 2D (X, Y) orthogonal curvilinear grids. Therefore all XY planes along Z direction are identical (the co-ordinates in the Z direction is independent of the other two), this leads to much fewer geometric quantities compared with fully 3D transform and the geometric quantities are only needed to be calculated on one XY plane. The non-zero $H_i(j)$ in the present study are $H_1(2)$, $H_2(1)$, $H_3(1)$ and $H_3(2)$ which can be computed numerically as follows:

$$H_1(2) = \frac{\Delta x_{j+1} - \Delta x_j}{\Delta x_{j+1/2} \Delta y_{j+1/2}} \tag{6}$$

$$H_2(1) = \frac{\Delta y_{i+1} - \Delta y_i}{\Delta x_{i+1/2} \Delta y_{i+1/2}} \tag{7}$$

$$H_3(1) = \frac{\Delta r_{i+1} - \Delta r_i}{\Delta x_{i+1/2} \Delta r_{i+1/2}} \tag{8}$$

$$H_3(2) = \frac{\Delta r_{j+1} - \Delta r_j}{\Delta y_{j+1/2} \Delta r_{j+1/2}} \tag{9}$$

where r in Equations (8) and (9) denotes radius when the third dimension is rotated. If the third direction is translated, $H_3(1)$ and $H_3(2)$ will be zero.

2.2. Numerical methods

The philosophy of LES is to compute directly the large-scale energy-dominate structures of turbulent motion while modelling only the remaining fine-scale eddies which are usually homogeneous and isotropic. The large-scale velocity components of the flow field are defined (separated from the small scales) by spatially filtering the governing equations. There are two school of thoughts with respect to filtering. It is called 'explicit filtering' if a filter such as a Gaussian one is applied to the equations. However, in many finite-difference computations, this filter is actually implemented implicitly through the grid's resolution and this is called 'implicit filtering'. This can be regarded as imposing a top hat filter and the local filter width in this case is equivalent to the local grid spacing. In explicit filtering for homogeneous turbulent flow the filter width can be kept constant along any spatial direction and the filtering operation is of a convolution type which has the convenient property that filtering and differentiation operations commute. For inhomogeneous flows the filter width should be a function of space because the average size of turbulent eddies varies in space. However, when the filter width varies the commutation between filtering and differentiation operations breaks down which leads to the governing equations essentially intractable for numerical solution. Some progress has been made in the development of nonuniform filters [15]. In addition, in complex geometry the governing equations in general co-ordinates are necessary which involves a complicated issue whether to transform the equations first then filter the equations in computational space or filter the equations first in physical space. It is argued by Jordan [16] that the recommended order-of-operations is to transform the equation system first, then filter the result. This sequence logically conforms the filter operation to the curvilinear field lines but requires representing the coefficient metrics as filter quantities.

Since the finite volume method with a staggered grid is used in the present study, and considering the above arguments, the implicit filtering approach is adopted here. The velocity components at the corresponding grid points are interpreted as the volume average. Any small scale (smaller than the mesh or control volume) motions are averaged out and have to be accounted for by a subgrid-scale model. However, note that it is impossible in this case to discuss the convergence properties (grid independent solution) of the LES equations because with every mesh refinement, more small scale eddies are resolved and strict convergence is only achieved in the limit of direct numerical simulation.

The spatial discretization used in the present study is second-order central differencing. While higher-order numerical schemes, generally speaking, are desirable and can be applied fairly easily in simple geometries, their use in complex configurations is rather difficult. In addition, it is essential that the numerical schemes for LES are both non-dissipative and conservative (not only mass and momentum but also kinetic energy conserving). These

requirements rule out the use of even higher-order upwind or upwind-biased schemes since they still produce too much numerical dissipation [9]. On the other hand, it is difficult, at least for incompressible flows, to construct high-order energy conserving schemes [17] and this is one of the reasons why the second-order central difference scheme on a staggered mesh is still so popular because it conserves global kinetic energy on uniform Cartesian meshes. Although this energy conservation property has not been proven for non-uniform meshes it is still likely that with increasing use of LES on body-fitted curvilinear grids for applications to flows of engineering interest in complex geometries the second-order central differencing scheme is going to be widely used.

Numerical schemes with unstructured mesh are very appealing for LES of complex engineering flows and there are a few groups in the world which are working on this, following the pioneering work by Jansen [18]. However, they appear to be too memory and/or CPU intensive at present for the relatively large number of mesh points needed for turbulence simulations in complex geometries.

With respect to time advancement, implicit schemes allow larger time steps to be used. However, they are more expensive because at each time step non-linear equations have to be solved. Furthermore, large time steps are unlikely to be used in LES in order to resolve certain time scales for accurate simulations of turbulence. Hence, explicit schemes seems to be more suitable for LES than implicit schemes and most researchers in LES use explicit schemes, of which the Adams–Bashforth scheme is a popular and robust one and is used in the present study. Since the time steps are usually small in LES so that it is not essential to use much higher-order schemes either.

The Adams–Bashforth scheme used in the current study is presented briefly as follows:

$$\frac{\hat{u}_i - u_i^n}{\Delta_i} = \frac{3}{2}H_i^n - \frac{1}{2}H_i^{n-1} + \frac{1}{2}\frac{\partial p^n}{\partial x_i} \tag{10}$$

$$\frac{u^{n+1} - \hat{u}_i}{\Delta t} = -\frac{3}{2}\frac{\partial p^{n+1}}{\partial x_i} \tag{11}$$

$$\nabla^2 p^{n+1} = \frac{2}{3\Delta t}\frac{\partial \hat{u}_j}{\partial x_j} \tag{12}$$

where $\hat{u}_i$ is the intermediate velocity and H_i denotes the contribution of convective and diffusive terms. Equation (10) is solved first to get the intermediate velocity $\hat{u}_i$, then the Poisson equation (12) for pressure derived by imposing the divergence free condition for the new velocity fields at $n+1$ time-level is solved to obtain pressure, finally the velocity filed at $n+1$ time-level is obtained from Equation (11).

2.3. *Multigrid Poisson solver*

Since explicit scheme is used to solve the momentum equations, the efficient solution of the Poisson equation of pressure plays a vital role in the overall computation efficiency of LES. Typically, the solution of pressure equation consumes 70% of the total CPU time. Multigrid method [19] is employed to speed up (for example, about 50% speed up has been achieved for a 180° bend square duct flow in the present study) the solution of the Poisson equation for pressure in the present study.

The logic of multigrid method lies in the fact that the iterative errors can be divided into two parts: high-frequency ones and low-frequency ones. The high-frequency errors can be removed more easily than the low-frequency ones through the common iterative method like Gauss–Siedel iteration. If several grid levels are used, the low-frequency errors on the fine grid become the high-frequency errors on the coarse grid and hence be removed relatively quickly.

A two-grid iterative method is as follows:

- On the fine grid, perform iterations with a method that gives a smooth error.
- Compute the residual on the fine grid.
- Restrict the residual to the coarse grid.
- Perform iterations of the correction equation on the coarse grid.
- Interpolate the correction to the fine grid.
- Update the solution on the fine grid.
- Repeat the entire procedure until the residual is reduced to the desired level.

2.4. Boundary conditions

The boundary conditions used are fairly standard and will be presented very briefly here. In LES specifying the inflow boundary conditions accurately is very difficult and will be discussed more below.

2.4.1. Inflow condition. Unlike the RANS computations where the inflow boundary conditions can be simply specified according to experimental data or other kind of information, for LES at the inflow planes, the values of three components of instantaneous velocity are required at each time step which are almost impossible to be obtained from any experimental data. For fully developed turbulent flows, the inflow conditions are usually specified in three ways. The first one is to specify the mean flow plus random perturbation. This is the easiest way but random disturbances are nothing like the real turbulence as they have no correlation either in space nor in time and have usually a flat spectrum similar to that of the white noise. Therefore, they decay rapidly and it takes certain distance downstream from the inflow boundary for a desired realistic turbulence to develop. However, in some cases the use of random noise at the inlet does not develop turbulence at all. This method makes it almost impossible to specify the inflow boundaries conditions with any required turbulence quantities such as shear stress or spectrum. The second method is to generate the instantaneous inflow velocity components in such a way that they are correlated and with required first, second moments and power spectrum. This is an ideal way of generating inflow boundary conditions as realistic turbulence can be provided and it is much cheaper compared with the third one. However, it is very difficult to generate the inflow velocity components with all the desired turbulence properties. It is possible to generate inflow turbulence with one or two properties but as far as we know there are not any methods available which can be used to generate inflow turbulence with all the desired characteristics such as intensity, shear stresses, length scales and power spectrum. Finally, one can use the so-called precursor simulation technique, which is basically to perform another simulation and store the data as the input for the required simulation. This can generate the most realistic turbulence information but the penalty is that it is too expensive.

2.4.2. Other boundary conditions. At outlet a convective boundary condition is employed. In wall bounded flows, the number of grid points required to resolve the boundary layer increases dramatically with Reynolds number. This near-wall resolution requirement, in many cases, could be the severest bottleneck in applying LES to flows of practical interest. As it is not absolutely necessary in many cases to resolve the wall layer some approximate boundary conditions, i.e. wall functions, can be applied on the walls. It is more difficult to apply wall functions in LES than in RNAS calculation and in the current study the approach by Schumann [20] is taken with slightly modification on calculating the mean friction velocity or wall shear stress. The mean wall shear stress in Schumann's model in the case of channel flow is equal to the driving mean pressure gradient. This implies that the mean driving pressure gradient should be known *a priori* which is quite restrictive. The mean wall shear stress in the current study is calculated in a sort of iterative way from the logarithmic law knowing the mean velocity at the nearest mesh point to the wall. This is described briefly as follows. Assuming that y is the direction normal to the wall

$$\tau_{12}|_{y=0} = \frac{\tilde{u}(x, \Delta y, z, t)}{\langle \tilde{u}(x, \Delta y, z, t) \rangle} \langle \tau_{12} \rangle \tag{13}$$

$$v|_{y=0} = 0 \tag{14}$$

$$\tau_{32}|_{y=0} = \frac{\tilde{w}(x, \Delta y, z, t)}{\langle \tilde{w}(x, \Delta y, z, t) \rangle} \langle \tau_{32} \rangle \tag{15}$$

where $\langle\,\rangle$ denotes time mean. Equations (13) and (15) simply state that the instantaneous wall shear stresses is in phase with the instantaneous velocity at the first grid point close to the wall; Assuming that the first grid point next to the wall is in the log-law region, $\langle \tilde{u}(x, \Delta y, z, t) \rangle$ satisfies the following log-law equation:

$$\langle \tilde{u}(x, \Delta y, z, t) \rangle = \frac{u_\tau}{\kappa} \left[\ln \left(\frac{u_\tau \Delta y}{\nu} \right) + c \right] \tag{16}$$

where $\kappa = 0.41$ is the von Karmann constant and c is another constant whose value is taken to be 2.3; $u_\tau = \sqrt{\tau_{12}/\rho}$ is the friction velocity, and the same treatment with $\langle \tilde{w}(x, \Delta y, z, t) \rangle$. In the simulation the wall functions are automatically switched on if y^+ at the first mesh point to the wall is greater than 11 otherwise a non-slip wall boundary condition is applied. However, it is worth pointing out that to ensure accuracy y^+ should be about 1 or smaller when a non-slip wall boundary condition is used.

The two sides in the spanwise direction can be treated as solid walls or periodic boundaries depending on the cases studied. The treatment of periodic boundary condition and the coupling of block interfaces is very similar. Figure 1 shows the periodic boundaries and the block interfaces, respectively.

Take u velocity as an example, the following relationship is applied:

$$u(1) = u(\mathrm{ni}); \;\; u(\mathrm{nip1}) = u(2)$$

It should be aware that this is valid only when the corresponding control volumes have the same geometric dimensions.

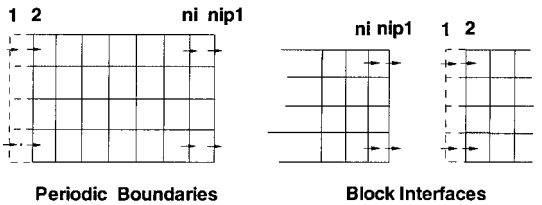

Figure 1. Periodic boundaries and block interfaces.

3. VALIDATION AND APPLICATIONS

Large eddy simulations of a channel flow, flow in a 180° bend square duct and in a typical dump diffuser geometry have been carried out using the numerical methods described above. The channel flow simulation has been carried out mainly as a validation of the code using the numerical techniques described and the results will be compared with available measurements by Wei and Willmarth [21] and LES results by Shah and Ferziger [22] under the same flow conditions. In order to test the curvilinear capability of the code a more complicated and difficult test case is chosen, i.e. the flow in a 180° bend square duct. The current numerical results will be compared with not only the experimental data by Chang *et al.* [23] but also the LES results using a collocated grid by Breuer and Rodi [24]. The dump diffuser flow simulation is an example of the use of these techniques in realistic practical engineering flow calculation, and comparison with the experimental data obtained also at Loughborough university will be presented.

3.1. Channel flow

The Reynolds number based on the half channel height and bulk velocity is 38 000. The size of the computational box is 2.5π (streamwise, x), 2 (normal, y) and 1.5π (spanwise, z). The mesh is uniform in the streamwise and spanwise direction, and stretched in the normal direction with a grid size of $64 \times 82 \times 82$ in the (x, y, z directions). The mesh is stretched in y direction and the $\Delta y_{\min}$ (first near wall cell) is about 1, justifying the use of a no-slip wall boundary condition.

Simulation started with randomly disturbed initial fields using periodic boundary conditions in both streamwise (the mass flow rate was imposed) and spanwise directions. It took roughly 50 000 steps to reach fully developed, statistically stationary flow state when total turbulent kinetic energy (spanwise averaged only) fluctuates around a certain value (not increasing or decreasing continuously) and then samples were collected every 10 steps to obtain time-averaged data. An ensemble of around 10 000 samples was collected to perform a rolling average (around 100 000 time steps, corresponding to around 15 flow-through or residence times).

Figure 2 shows the streamwise mean velocity profile and it can be seen that the current numerical results compare quite well with the LES results obtained with the Smagorinsky subgrid scale model by Shah and Ferziger [22]. The predicted mean velocity matches the theoretical log-law curve well in the near wall region which indicates that the mesh resolution in the near wall region is fine enough. Further away from the wall ($y^+ > 200$) the log-law velocity profile is well captured. However, both the current LES results and the LES results

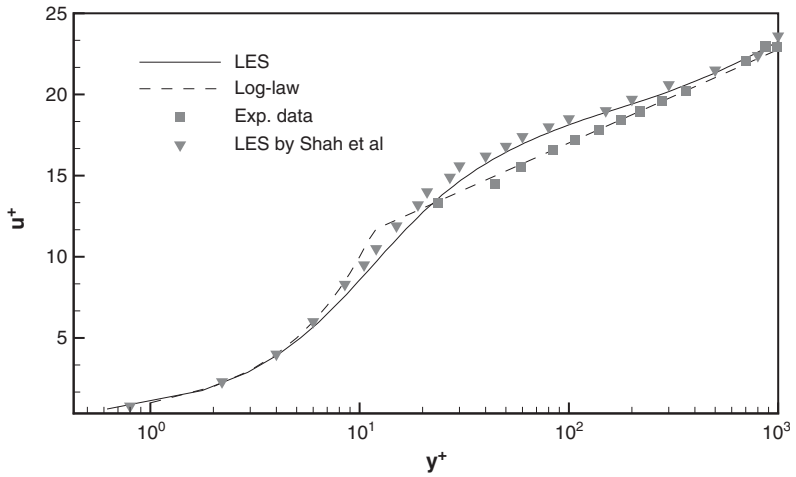

Figure 2. Mean streamwise velocity profile.

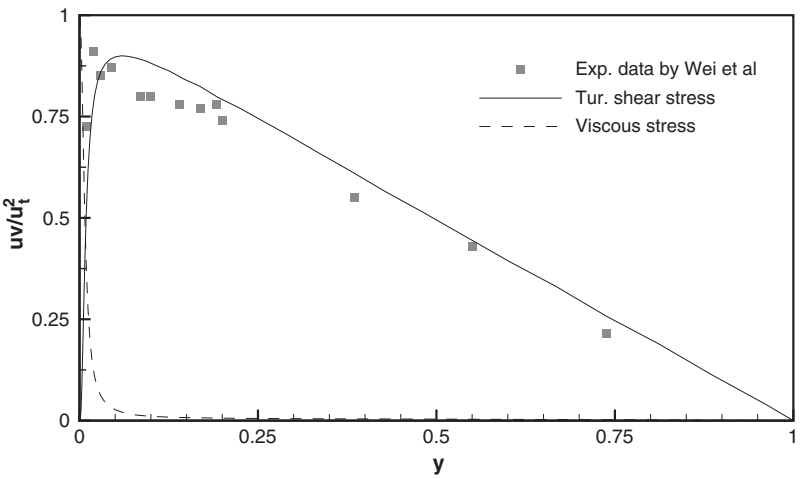

Figure 3. Mean shear stress profile.

by Shah and Ferziger [22] show a bulge in the region $20 < y^+ < 300$ compared with the log-law profile. This may be due to the under-prediction of the skin friction by the conventional Smagorinsky model which causes the velocity profile to rise above the log-law profile.

The comparison between the predicted shear stress (normalized by u_τ^2) and the experimental data is shown in Figure 3 and as expected the predicted shear stress (resolved Reynolds stress plus the subgrid stress) is a straight line away from the walls, indicating that the flow is fully developed and the average Reynolds shear-stress has attained the equilibrium shape. It also indicates that the total averaging time is sufficient (adequate samples have been collected). In the near wall region the viscous stress are significant, and they, together with the turbulent

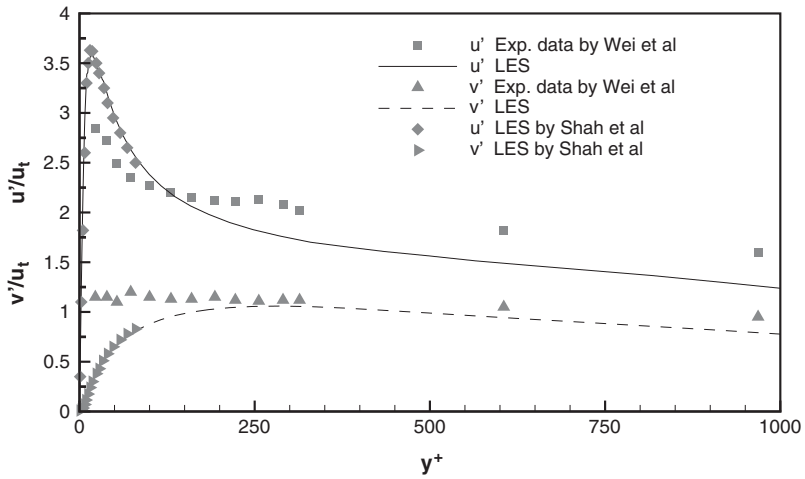

Figure 4. Profiles of normal stresses, u-rms and v-rms.

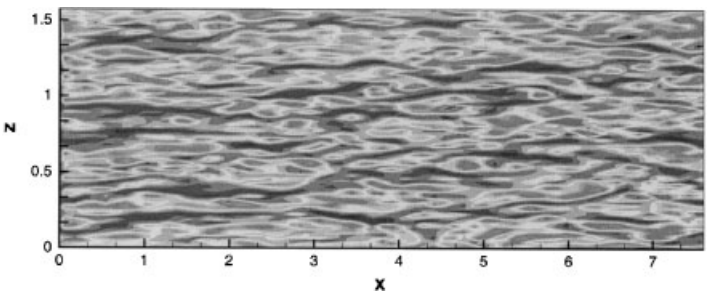

Figure 5. Contours of u' at $y^+ = 11.3$.

shear stress, balance the mean pressure gradient. The comparison with the experimental data [21] is reasonably good despite the fact that the experimental data are a little bit scattered when approaching the wall.

The turbulent normal stresses normalized by u_τ are shown in Figure 4. As can be seen from the figure that the peak value of the predicted normal stress u' is about 15% larger than the experimental data [21]. The predicted wall normal stress v' goes down smoothly to zero towards the wall whereas the experimental data remain flat all the way till close wall region which seem to be unrealistic. At very close wall region there are no experimental data since it is very difficult, if not impossible, to take measurements in the very close wall region. The current numerical results compare very well with the LES results obtained with the Smagorinsky model by Shah and Ferziger [22] in the near wall region as shown in the figure.

It has been well established that in wall bounded turbulent flows the high- and low-speed streaks in the near wall region alternate in the spanwise direction. This well-known streaky structure can be clearly seen from Figure 5 which shows the contour of u' in the (x,z) plane

at $y^+ = 11.3$. This indicates the resolution used in the current simulation, especially in the spanwise dimension is good enough.

3.2. *Flow in a 180° bend square duct*

The Reynolds number based on the hydraulic diameter and the bulk mean velocity is about 56 700 and the ratio of the mean curvature to the hydraulic diameter is 3.35. More details can be found in Reference [23]. The fully inhomogeneous flow in such a 180° duct cannot be simulated by spectral or Cartesian finite-difference methods and the current curvilinear grid consists of $121 \times 66 \times 66$ mesh points, which are roughly the same mesh points as in Breuer and Rodi's LES simulation [24]. The computational domain includes an upstream inlet and a downstream outlet, tangent to the 180° bend, of three hydraulic diameters. The precursor method as mentioned before was used to generate the inlet conditions.

Statistics are gathered by averaging in time only as there is no homogeneous directions after the simulation is in its fully developed, statistically stationary state. The simulation is run for 70 000 time steps to reach the statistically stationary state, and the results presented below are then gathered over a further 200 000 time steps (around 2 s, corresponding to around 10 flow-through or residence times) with a sample taken every 10 time steps (20 000 samples).

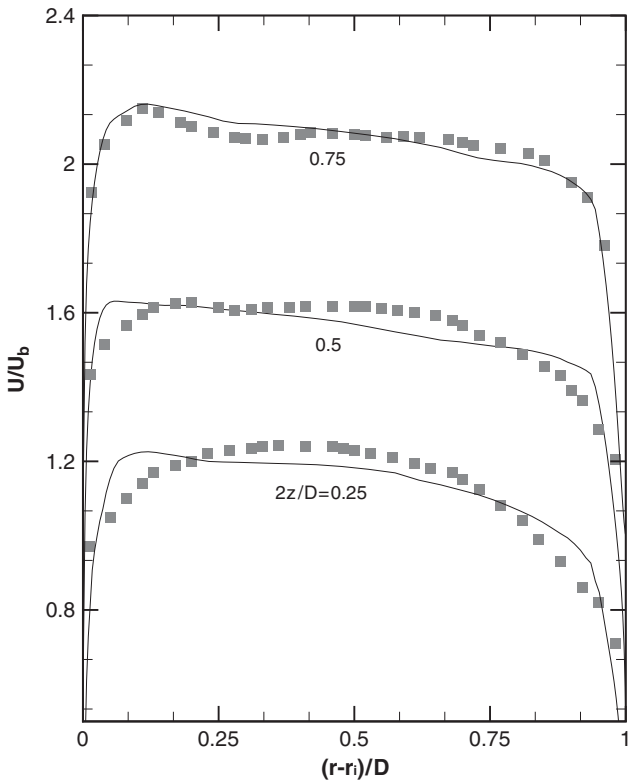

Figure 6. Mean streamwise velocity profiles at 3° station, solid line: LES; symbols: Exp. data.

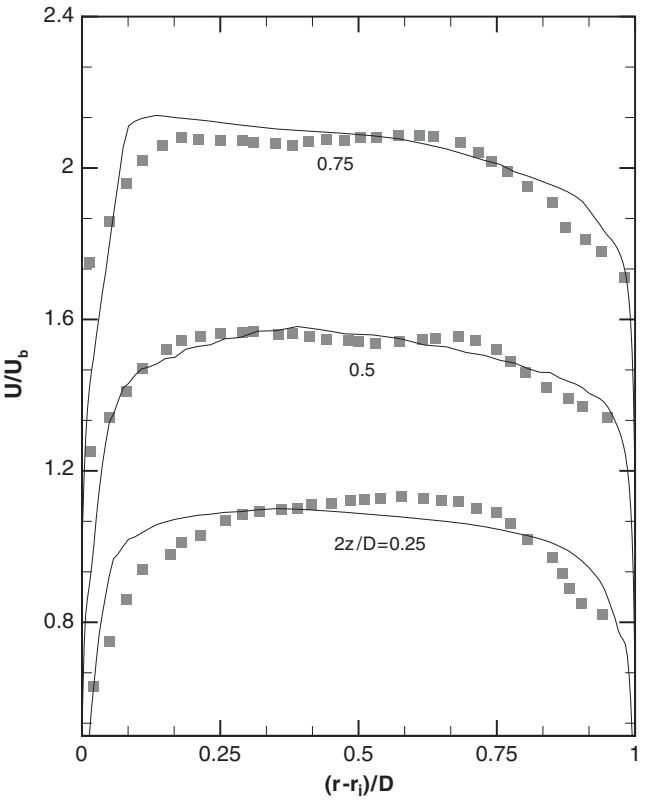

Figure 7. Mean axial velocity profiles at 45° station, solid line: LES; symbols: Exp. data.

Figure 6 shows profiles of mean streamwise velocity at $\theta = 3°$ at different heights. Overall agreement between the numerical results and the experimental data at all three different heights is good. Both the experimental data and the LES results clearly indicate that even at such an earlier stage of flow going inside the bend section all the profiles are already different from the normal channel flow situation, showing their maximum values displaced towards the inner wall due to the favourable streamwise pressure gradient there.

The comparison between the numerical results and the experimental data at $\theta = 45°$ is shown in Figure 7 and the overall agreement is quite good too. At the near wall plane, $2z/D = 0.25$ (z is the normal distance and D is the height of the square duct), the LES predictions still show similar profile to that at $\theta = 3°$ station. However the experimental data indicate that the profile is slightly different from that at $\theta = 3°$ station, with the maximum value shifted towards the outer wall. At $2z/D = 0.5$ and 0.75 the agreement is better although it seems that the experimental data show a tiny peak towards the outer wall which the LES results fail to capture. This could be due to the secondary motions and the current mesh resolution may not be fine enough to simulate it properly.

Figure 8 shows profiles of mean streamwise velocity at $\theta = 90°$, compared with both the experimental data and the LES results by Breuer and Rodi [24]. The agreement between the

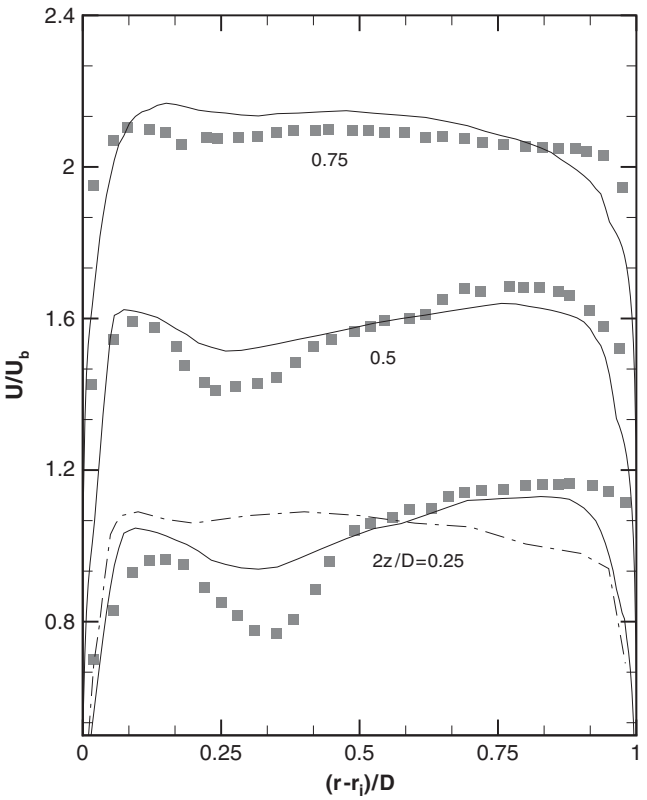

Figure 8. Mean axial velocity profiles at 90° station, solid line: LES; symbols: Exp. data; dashed line: LES by Breuer and Rodi.

current LES results and the experimental data is not as good as in the previous two stations. At $2z/D = 0.25$ and 0.5 the experimental data indicate double peaks clearly, one near the inner wall and the other near the outer wall, and after the peak near the inner wall there is a big trough followed immediately. This kind of behaviour of velocity profiles are mainly due to the secondary motions which are possibly the strongest at this station. The current LES results show the correct trends with two peaks predicted but under-predicted the trough. However, it can be seen clearly that the current numerical results compare better than the LES results by Breuer and Rodi [24]. Both simulations use roughly the same mesh points but it is hard to draw any firm conclusion based on only very limited comparisons.

3.3. Dump diffuser flow

As an example of the use of these techniques in practical, complex engineering geometry, we present results from the simulation of the flow in a typical dump diffuser region of gas turbine combustor. This flow involves separation and reattachment which is very difficult, if not impossible, to predict by a conventional turbulence model.

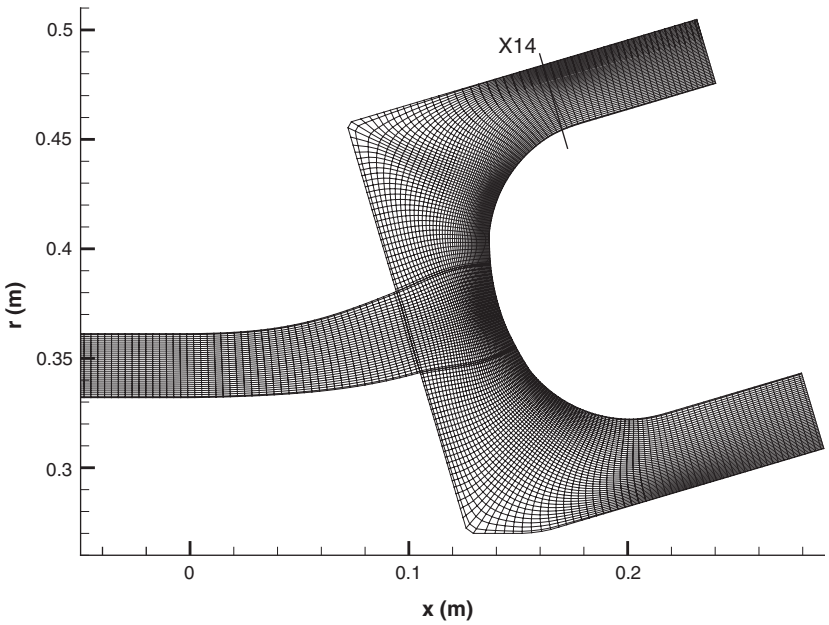

Figure 9. Computational domain and the mesh.

The overall geometry and meshing is shown in Figure 9. The simulations were performed using the techniques outlined in previous sections on both a coarse mesh with 110 000 grid points and a much finer mesh with about 800 000 grid points. The mean flow and turbulence quantities are broadly similar and it has been found that inflow boundary conditions have a stronger influence on the results than the mesh refinement so that the inflow boundary conditions (data) are generated here using the precursor simulation technique. The Reynolds number based on the pre-diffuser duct height is 65 000 and the results presented below are at X14 station as shown in Figure 9.

Statistics are gathered by averaging in time and also over the span direction once the simulation is in its fully developed, statistically stationary state. The simulation is run for 90 000 time steps to reach the statistically stationary state, and the results presented below are then gathered over a further 150 000 time steps (around 0.9 s, corresponding to around 60 flow-through or residence times) with a sample taken every 5 time steps (30 000 samples).

Figure 10 shows contours of mean and instantaneous axial velocity which illustrate that the instantaneous flow field is very different from the averaged one. In particular, large differences can be observed between the instantaneous and averaged recirculation region size, with large scale movement of the instantaneous re-attachment points as the instantaneous flow fields are different and changing all the time. The mean flow field will not change if averaged long enough (enough samples collected).

Figure 11 shows the predicted mean axial and transverse velocity profiles (normalized by the bulk velocity) compared with experiment at station X14 (location of X14 is shown in Figure 9). The profiles are plotted against normalized co-ordinate r starting from 0 (inner

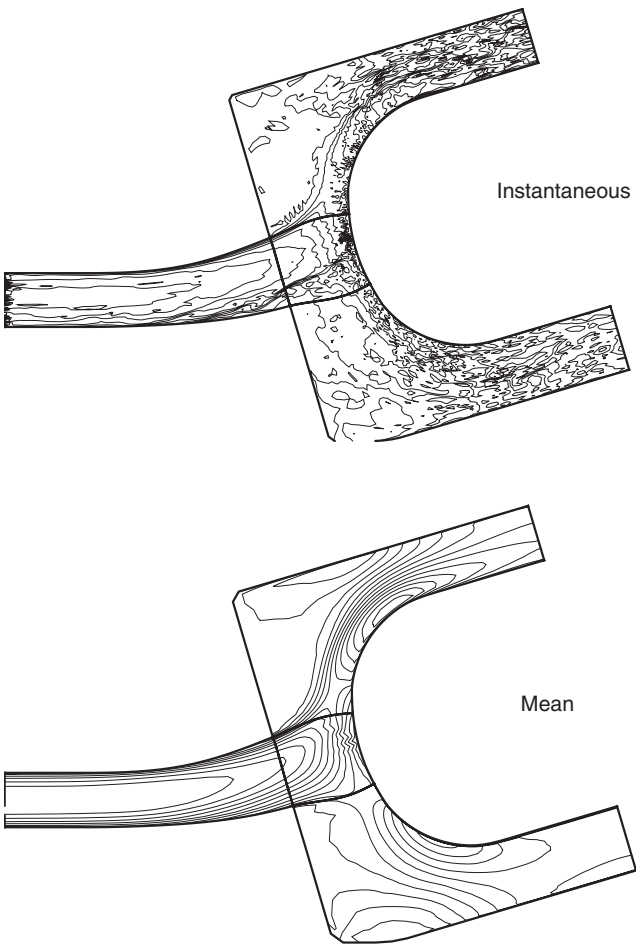

Figure 10. Contours of mean and instantaneous axial velocity.

wall) to 1 (outer wall). It can be seen that a good agreement of mean axial velocity has been obtained between the LES results and the experimental data. Both the simulation and the experiments show that a small reverse flow region still exists at X14. However, the predicted axial velocity profile by a RSM (steady axisymmetric 2D) does not capture this reverse flow region. The agreement of mean transverse velocity between the LES and the experiment is also quite good while the RMS prediction is much lower compared with the experimental data.

All three turbulence rms values at the same location X14 (normalized by the bulk velocity) are shown in Figure 12. The predicted u', v' by LES and the experimental data compare reasonably well in terms of both the magnitude and the profile shape apart from that the LES results show a peak near the inner wall but no experimental data available in this region so close to the wall whereas the RSM results are only about 50% of the measured values everywhere. The predicted w' by LES also agrees well with the experimental data, especially

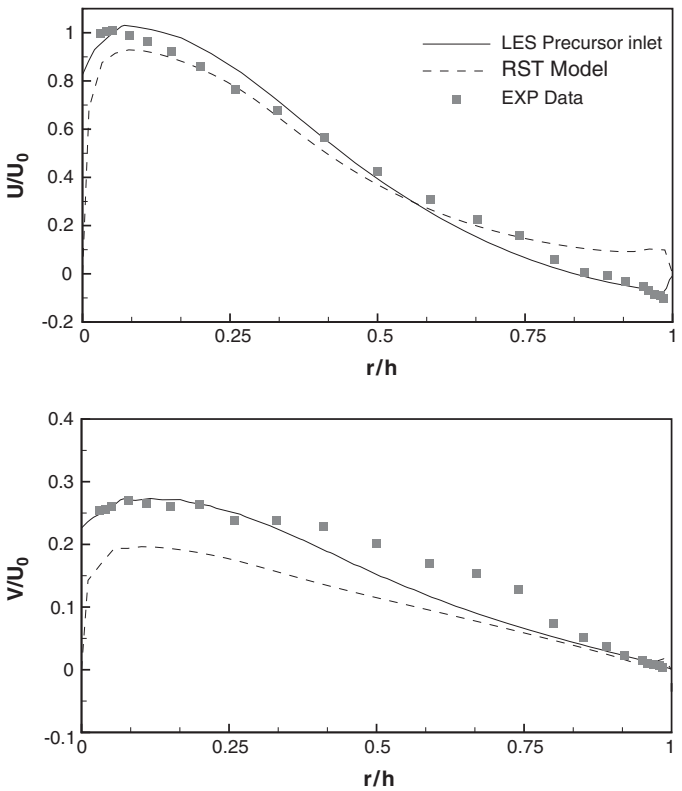

Figure 11. Mean axial and normal velocity profiles.

the peak value near the outer wall which the RSM failed to predict completely. The profile shape predicted by the RSM is quite different from the measured profile and the predicted value is less than 50% of the measured value. We believe that the peak of w' profile near the outer wall is mainly due to large scale unsteady motion in this region associated with the movement of the instantaneous reattachment points, which any turbulence models based on RANS approach might fail to capture. Further details of the flow physics, structures etc. will be given elsewhere.

4. CONCLUSIONS

Numerical methods for performing large-eddy simulations using general curvilinear orthogonal co-ordinates have been described. Several key issues in LES such as inlet flow boundary conditions, filtering, choice of velocity components (cartesian or contravariant) have been discussed. The numerical methods have been evaluated using a fully developed channel flow as a standard test case and an overall good agreement has been obtained between the LES results and the experimental data for both the mean velocity and turbulence quantities. A more difficult flow problem, a reasonably high Reynolds number square duct flow with a 180°

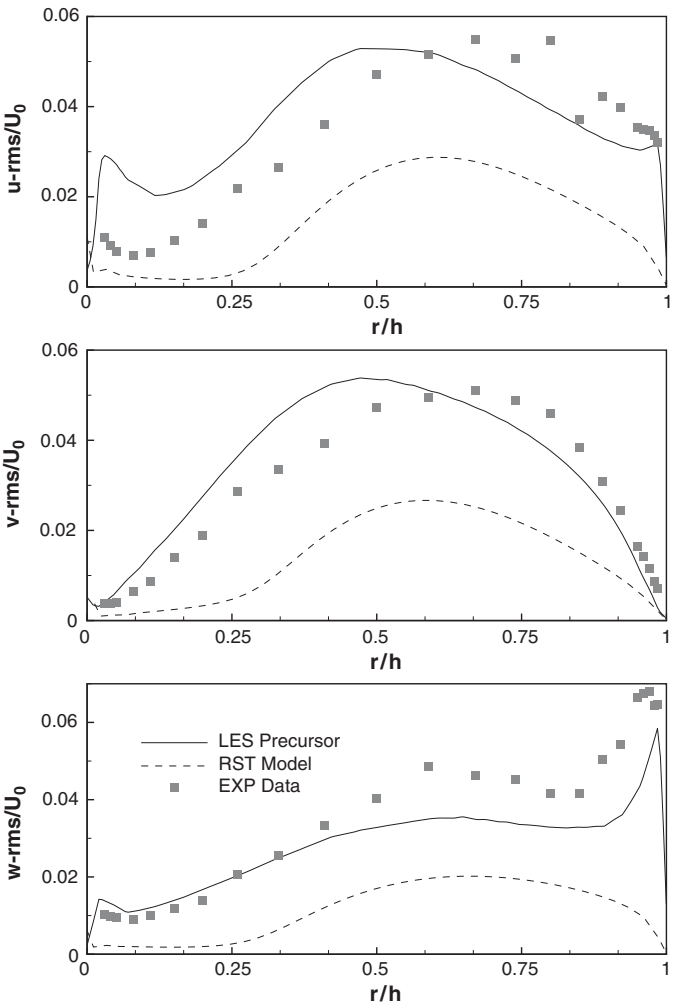

Figure 12. Profiles of u-rms, v-rms and w-rms at X14.

bend was chosen to examine the performance of the current LES methodology. The overall agreement between the LES predictions and the experimental data is quite good. There are some differences mainly at $\theta = 90^\circ$ station and the secondary motion appears to be responsible for the discrepancies as the mesh resolution used in the current study is not fine enough to capture the secondary motion accurately.

A much more complicated and realistic engineering flow in a typical dump diffuser region of gas turbine combustor has then been simulated using the numerical techniques described. The predicted mean velocity and turbulence quantities by LES compare well with the measured values whereas a RSM performed badly in this complex flow, failing to capture flow dynamics due to large scale unsteady motions indicated by the measurements which LES has successfully predicted. Further detail analysis of the LES data in this case to shed light on flow physics and structures will be presented elsewhere.

The LES techniques presented in the paper have been proven robust, efficient and reliable after applying to three different flow cases with good results obtained compared with experimental data.

ACKNOWLEDGEMENTS

This work was carried out in the University Technology Centre in Combustion Aerodynamics at Loughborough University. The authors would like to thank colleagues at Loughborough University and Rolls-Royce for advice and comments and in particular Drs A.P. Manner and S. Zheng for developing an earlier version of the LES code.

REFERENCES

1. Antonopoulos-Domis M. Aspects of large eddy simulation of homogeneous isotropic turbulence. *International Journal for Numerical Methods in Fluids* 1981; **1**:273–290.
2. Moin P, Kim J. Numerical investigation of turbulent channel flow. *Journal of Fluid Mechanics* 1982; **118**: 341–377.
3. Voke PR, Yang Z. Numerical study of bypass transition. *The Physics of Fluids* 1995; **7**:2256–2264.
4. Kaltenbach H-J, Fatica M, Mittal R, Lund TS, Moin P. Study of flow in a planar asymmetric diffuser using large-eddy simulation. *Journal of Fluid Mechanics* 1999; **390**:151–185.
5. Yang Z, Voke PR. Large-eddy simulation of boundary layer separation and transition at a change of surface curvature. *Journal of Fluid Mechanics* 2001; **439**:305–333.
6. Eggels EGM, Nieuwstadt FTM. Large-eddy simulation of turbulent flow in an axially rotating pipe. *Proceedings, 9th Symposium on Turbulent Shear Flows* 1993; P310-1–P310-4.
7. Yang Z, McGuirk JJ. LES of rotating turbulent pipe flow with two sub-grid scale models. In *Turbulence and Shear Flow Phenomena-1*, Banerjee S, Eaton J (eds). Begell House, Inc.: New York, USA, 1999; 863–868.
8. Tafti DK, Vanka SP. A three-dimensional study of flow separation and reattachment on a blunt plate. *The Physics of Fluids* 1991; **A3**:2887–2909.
9. Moin P. Progress in large-eddy simulation of turbulent flows. *AIAA paper 97-0749*, 1997.
10. Lesieur M, Metais O. New trends in large-eddy simulations of turbulence. *Annual Review of Fluid Mechanics* 1996; **28**:45–82.
11. Morinishi Y, Lund TS, Vasilyev OV, Moin P. Fully conservative higher order finite difference schemes for incompressible flow. *Journal of Computational Physics* 1998; **143**:90–124.
12. Yang Z, Voke PR. Large-eddy simulation of separated leading-edge flow in general co-ordinates. *International Journal for Numerical Method in Engineering* 2000; **49**:681–696.
13. Pope S. The calculation of turbulent recirculating flows in general orthogonal coordinates. *Journal of Computational Physics* 1978; **26**:197–217.
14. Smagorinsky J. General circulation experiments with the primitive equations. I. The basic experiment. *Monthly Weather Review* 1963; **91**:99–164.
15. Van Der Ven H. A family of large eddy simulation (LES) filters with nonuniform filter widths. *The Physics of Fluids* 1995; **7**:1171–1172.
16. Jordan SA. A large-eddy simulation methodology in generalized curvilinear coordinates. *Journal of Computational Physics* 1999; **148**(2):322–340.
17. Morinishi Y. Conservative properties of finite difference schemes for incompressible flow. *Annual Research Brief*, Center for Turbulence Research, NASA Ames/Stanford University, 1995; 121–132.
18. Jansen K. Large-eddy simulation of flow around a NACA 4412 airfoil using unstructured grids. *Annual Research Briefs 1996*, Center for Turbulence Research, Stanford University and NASA Ames, 1996; 225–232.
19. Zeng S, Wesseling P. Multigrid solution of the incompressible Navier–Stokes equations in general coordinates. *SIAM Journal on Numerical Analysis* 1994; **31**:1764–1784.
20. Schumann U. Subgrid scale model for finite difference simulations of turbulent flows in plane channels and annuli. *Journal of Computational Physics* 1975; **18**:376–404.
21. Wei T, Willmarth WW. Reynolds-number effects on the structure of a turbulent channel flow. *Journal of Fluid Mechanics* 1989; **204**:57–95.
22. Shah KB, Ferziger J. A new non-eddy viscosity sub-grid scale model and its application to channel flow. *Annual Research Briefs*, Center for Turbulence Research, Stanford University, 1995.
23. Chang SM, Humphrey JAC, Modavi A. Turbulent flow in a strongly curved U-bend and downstream tangent of square cross-sections. *Physico Chemical Hydrodynamics* 1983; **4**:243–269.
24. Breuer M, Rodi W. Large-eddy simulation of turbulent flow through a straight square duct and a 180° bend. In *Direct and Large-Eddy Simulation I*, Voke PR *et al.* (eds). Kluwer Academic Publishers: Dordrecht, 1994; 273–285.

